

Structure of the Subduction System in
Southern Peru from Seismic Array Data

Thesis by
Kristin Phillips-Alonge

In Partial Fulfillment of the Requirements for the Degree
of
Doctor of Philosophy



CALIFORNIA INSTITUTE OF TECHNOLOGY

Pasadena, California

2013

(Defended November 21, 2012)

© 2013
Kristin Phillips-Alonge
All Rights Reserved

ACKNOWLEDGEMENTS

Robert Clayton

Younghee Kim

Richard Guy

Paul Davis

Igor Stubailo

Steve Skinner

Hernando Tavera

Victor Aguilar

Laurence Audin

Tectonics Observatory at Caltech

NSF

ABSTRACT

Southern Peru represents a subduction transition region from normal subduction in the southernmost part of Peru to flat slab subduction in central Peru. In order to learn more about the structure of southern Peru, causes of flat slab subduction, and the nature of the transition from normal to flat slab subduction, we installed three seismic arrays utilizing a total of about 100 broadband stations. The first installed array samples the normal subduction region, while the second samples the transition from normal to flat subduction, and the third samples the flat slab region near where the Nazca Ridge is presently subducting. Data from teleseismic events greater than 30 degrees distance from Peru was analyzed using the receiver function method that makes use of P to S converted phases at interfaces such as the Moho to provide information about the structure directly beneath each station. A strong signal from the Moho was observed for each array and was found to have a maximum depth of around 75 km beneath the Altiplano. The average crustal V_p/V_s ratio was also estimated and was found to have an average value of around 1.75 beneath the Altiplano. The shape of the slab was also clarified for the three arrays. The transition from normal to flat slab subduction appears to be a contortion rather than a break in the slab. In addition to those signals, a positive impedance midcrustal signal at about 40 km depth was widely observed for stations on the eastern side of the arrays. The midcrustal signal is indicative of a velocity increase in the lower crust and is suggested to be an observation of the underthrusting Brazilian shield which would have implications for the timing of uplift in the Andes. Finite difference modeling with velocity models that include a midcrustal structure produces synthetics which are consistent with receiver function observations. Receiver function results and other related methods provide a simple way of making direct observations of key structural interfaces and the current state of the subduction system which has relevance in studies of the tectonic evolution of the region and estimations of causes of flat slab subduction.

Table of Contents

Table of Figures and Illustrations.....	vii
Nomenclature	vii
<i>Chapter 1: Introduction and Summary</i>	1
Chapter 1 References	7
<i>Chapter 2: Normal Subduction Region</i>	10
Structure of the Subduction System in Southern Peru.....	10
From Seismic Array Data.....	10
Abstract.....	10
2.1. Introduction	11
2.2 Data, Methods, and Results	15
2.2.1 Receiver Functions.....	15
2.2.1.1 Receiver Function Results.....	20
2.2.1.2 Receiver Function Waveform Modeling.....	24
2.2.2 P-Wave Tomography	30
2.3 Discussion.....	33
2.3.1 Crustal Thickness	33
2.3.2 Midcrustal Structure	35
Conclusions	38
Acknowledgements:	39
Chapter 2 References	39
<i>Chapter 3: Subduction Transition and Flat Slab</i>	45
Structure of the Subduction Transition Region from Seismic.....	45
Array Data in Southern Peru	45
3.1. Introduction	46
3.2. Methods	50
3.2.1 Stations and Data.....	50
3.2.2 Receiver Functions.....	52
3.2.3 Finite Difference Modeling.....	54
3.3. Results.....	56
3.3.1 Line 2 Results: Transition From Normal to Flat Slab Subduction	56
3.3.2 Line 3 Results: Flat slab region	59
3.4. Discussion.....	63
3.4.1 Moho Depth and Vp/Vs.....	63
3.4.2 Slab Structure	65
3.4.3 Nazca Ridge and Causes of Flat Slab Subduction	70
Chapter 3 References	76
<i>Chapter 4: Methods and Other Results</i>	84
4.1: Field Work in Peru	84
4.1.1 Installation Procedure.....	85
4.1.2 Second and Third Arrays.....	86
4.2: Processing Methods and Receiver Function Methods	87

4.2.1: Processing procedure	91
4.2.2 Deconvolution methods	92
4.2.2.1 Frequency Domain Deconvolution.....	92
4.2.2.2. Time Domain Deconvolution.....	93
4.3 Phases used for RFs.....	99
4.3.1. P, PP, and PKP	99
4.3.2. S wave RFs.....	103
4.5 Transverse Receiver Function Components.....	107
4.6 Imaging Methods (Backprojection, CCP)	117
4.7 Finite Difference Modeling	120
4.8 Local Events and Future Study.....	123
4.8.1. Local Receiver Functions.....	126
4.8.2. Precursors to pP or sS.....	129
4.8.3. Modeling Local Events	135
4.8.4. Future Work: Determination of EQ Loc. and Focal Mechanisms.....	143
4.9 Summary and Conclusions.....	145
Chapter 4 References	147
Appendix A Chapter 2 Supplementary Figures	152
Appendix B Chapter 3 Supplementary Figures.....	157
Appendix C Chapter 4 Supplementary Figures.....	163
Bibliography	187

Table of Figures and Illustrations

Figure 1.1 Map of Peru.....	2
Figure 2.1 Line 1 tectonic settings	12
Figure 2.2: Local seismicity	14
Figure 2.3: Location of events.....	16
Figure 2.4: Data example.....	17
Figure 2.5: Line 1 receiver function.....	18
Figure 2.6 Stacking method.....	19
Figure 2.7 P/PP receiver function image, all directions, upper 120km.....	21
Figure 2.8: Line 1 P/PP RF, Moho and Vp/Vs results	22
Figure 2.9: Line 1 PKP receiver function image	24
Figure 2.10: Finite difference modeling.....	26
Figure 2.11: Comparison of data and synthetic results.....	27
Figure 2.12: Local event FD waveform modeling.....	29
Figure 2.13 Tomography	31
Figure 2.14 Checkerboard test.....	32
Figure 2.15 Gravity results	34
Figure 2.16 Line 1 model	38
Figure 3.1 Array map.....	49
Figure 3.2 Lines 2 and 3 seismicity cross sections	51
Figure 3.3 Line 2 results	55
Figure 3.4 Line 2 CCP plot.....	57
Figure 3.5 Line 2 RF migration.....	58
Figure 3.6 Line 3 RF image.....	59
Figure 3.7 Line 3 CCP and PKP image	60
Figure 3.8 Line 3 FD modeling	61
Figure 3.9 Lines 2 and 3 Moho and Vp/Vs results	62
Figure 3.10 Moho and slab models in 3D.....	67
Figure 3.11 Comparison of FD models and synthetics for all arrays.....	69
Figure 3.12 Comparison of normal and flat slab images.....	71
Figure 3.13 Seismicity and elevation comparison, Flat/Normal subduction regions	73
Figure 4.1 Station installation.....	86
Figure 4.2 Data from the Sandwich Islands on 12/08/2010	87
Figure 4.3 Processing methods, filtering	89
Figure 4.4 One versus two second filtered receiver functions	91
Figure 4.5 Time versus frequency domain deconvolution, line 3.....	94
Figure 4.6 Time versus frequency domain from CCP stacks.....	95
Figure 4.7 Time versus frequency domain receiver functions for 12/08/2010.....	97
Figure 4.8 PG40 time and frequency domain deconvolution.....	98
Figure 4.9 PG50 frequency versus time domain deconvolution	99
Figure 4.10 PE46 receiver functions, all phases (P, PP, and PKP).....	101
Figure 4.11 Comparison of P/PP images with PKP for Line 1	103
Figure 4.12 S wave RFs, Line 1	105
Figure 4.13 Stacking for Moho and Vp/Vs for PG05.....	107

Figure 4.14 Radial and transverse receiver functions for PF25	109
Figure 4.15 Radial and transverse receiver functions for PF37	110
Figure 4.16 Transverse RF stacks for PF25 from different azimuthal directions.....	111
Figure 4.17 Transverse RF stacks from the NW and SE for PF42	112
Figure 4.18 Stations PF42 and PF43 axis of symmetry in transverse RFs	113
Figure 4.19 Stations PF29 and PF31 symmetry axis	114
Figure 4.20 Stations PF23 and PF24 symmetry axis	115
Figure 4.21 Stations PF12 and PF13 symmetry axis.....	116
Figure 4.22 CCP stacks from each azimuthal direction for Line 3	1177
Figure 4.23 Backprojection for station PE46	119
Figure 4.24 Image for Line 1 based on CCP stacks	120
Figure 4.25 Large earthquakes near arrays during time of array operation	124
Figure 4.26 Deep events which can be used for local receiver functions	125
Figure 4.27 Processing of local receiver function on 11/22/2011.....	127
Figure 4.28 Local RF bandpassed to 2 sec. for Line 1, 2011/11/22.....	128
Figure 4.29 Local RF, 2011/11/22, bandpassed to 2 Hz	129
Figure 4.30 Large and deep events used for analysis of pP and sS precursors.....	130
Figure 4.31 Precursor to pP phase from 08/26/2008 event in N. Peru.....	132
Figure 4.32 Stack to find precursors to sS phase for event on 07/12/2009.....	133
Figure 4.33 More checks for pP precursors in Peru events	134
Figure 4.34 Data from 7/12/2009 bandpassed to 1 and 10 sec.....	135
Figure 4.35 Data from 9/05/2009 bandpassed to 1 and 10 sec.....	136
Figure 4.36 Data from 9/30/2009 bandpassed to 1 and 10 sec.....	137
Figure 4.37 Structural models for southern Peru	138
Figure 4.38 Finite difference synthetics for 2009/07/12	140
Figure 4.39 Finite difference synthetics for 2009/09/05	141
Figure 4.40 Finite difference synthetics for 2009/09/30	142
Figure 4.41 CMT solutions for 10/28/2011	1444
Figure A.1 PKP receiver functions	152
Figure A.2 P wave velocity models	153
Figure A.3 PKP versus P/PP slab.....	154
Figure A.4 Synthetic RF image.....	155
Figure A.5 Brazilian Shield/Line 1 model	156
Figure A.6 Initial model of Sheild.....	156
Figure B.1 Midcrustal signal	157
Figure B.2 Different slab models for Line 2.....	158
Figure B.3 Seismicity across Nazca Ridge	159
Figure B.4 Migrated images of Lines 1 and 3, interpreted.....	161
Figure B.5 RF migrations of Lines 1 and 3, uninterpreted.....	162
Figure C.1 The team	163
Figure C.2 Obtaining wireless connectivity.....	164
Figure C.3 Wireless links between sites	165
Figure C.4 Installation procedure	166
Figure C.5 Field challenges	167
Figure C.6 PF11 transverse RFs.....	168

Figure C.7 PF11 Transverse RFs, stacks from NE/SW and NW/SE.....	169
Figure C.8 Transverse RFs for PF12.....	170
Figure C.9 Transverse RFs for PF12, stacks/average for NW/SE	171
Figure C.10 Transverse RFs for PF13.....	172
Figure C.11 Transverse RFs for PF13, stacks/average for NE/SW	173
Figure C.12 Transverse RFs for PF23.....	174
Figure C.13 Transverse RFs for PF24.....	175
Figure C.14 Transverse RFs for PF29.....	176
Figure C.15 Transverse RFs for PF37.....	177
Figure C.16 Transverse RFs for PF37, stacks/averages for NE/SW and NW/SE	178
Figure C.17 Transverse RFs for PF39.....	179
Figure C.18 Transverse RFs for PF06.....	180
Figure C.19 Transverse RFs for PF07.....	181
Figure C.20 Radial and transverse RFs for PG27.....	182
Figure C.21 Radial and transverse RFs for PG40.....	183
Figure C.22 Radial and transverse RFs for PG42.....	184
Figure C.23 Figure 4.28, no interpretive lines	185
Figure C.24 Figure 4.29, no interpretive lines.	186

NOMENCLATURE

Subduction. Describes the movement of two tectonic plates in which a denser plate is forced beneath the lithosphere of a less dense plate

Normal subduction. Subduction in which the descending plate subducts at an intermediate angle close to 30 degrees.

Flat slab subduction. Subduction in which the descending plate subducts at a very shallow angle of less than 10 degrees for a portion of the subduction length. For example a plate which initially starts off subducting at a steep angle near the trench but flattens out to subduct almost horizontally beneath the overriding plate for a distance of several hundred kilometers before resuming subduction at a steeper dip angle would be considered flat slab subduction.

Underthrusting. A process during compression in which one rock body is thrust beneath another relatively stable rock structure.

Shield. Typically refers to exposed precambrian igneous and metamorphic rocks that form the stable interior of the continent

Moho. Short for Mohorovičić Discontinuity, the boundary between the crust and mantle marked by a seismic velocity increase

Tectonic plate/slab. Consists of lithosphere which is able to move on top of the viscous asthenosphere and interacts with other plates in a variety of tectonic settings such as subduction zones, strike slip regions, or divergent settings. A tectonic plate or slab includes continental or oceanic crust as well as mantle lithosphere. When used in the context of receiver functions, “slab” or “slab signal” is sometimes used to reference the subducting oceanic crust which is marked by receiver function pulses. However the subducting plate is understood to include the full lithosphere.

Chapter 1: Introduction and Summary

The following chapters provide details of the methods, analysis, results, and discussion of seismic data collected by arrays of seismic stations installed in southern Peru. Each chapter is structured as a self-contained paper and will have its own set of references at the end. The second chapter is in press with *Journal of Geophysical Research-Solid Earth*, while the third chapter was recently submitted to *Geophysical Journal International*.

The subduction style of the Nazca plate beneath South America varies along strike from areas of “normal subduction” where the slab dips at angles around 25° - 30° , to areas of flat slab subduction where the Nazca plate subducts at an angle less than 10° beneath South America, as observed from seismicity in the Wadati-Benioff zone. Areas of normal subduction include southern Ecuador ($\sim 0^{\circ}$ - 2° S), southern Peru/northern Chile ($\sim 15^{\circ}$ - 27° S), and southern Chile ($\sim 33^{\circ}$ - 45° S). Areas of flat slab subduction include central and northern Peru (2° - 15° S), central Chile ($\sim 27^{\circ}$ - 33° S) and central Ecuador (0° - 2° N) (Barazangi and Isacks 1976). Southern Peru represents a transition from normal to flat slab subduction. Three seismic arrays were arranged roughly in the shape of a box to sample the region of normal subduction (perpendicular to the trench), transition from normal to flat slab subduction (parallel to the trench), and region of flat slab subduction (perpendicular to the trench).

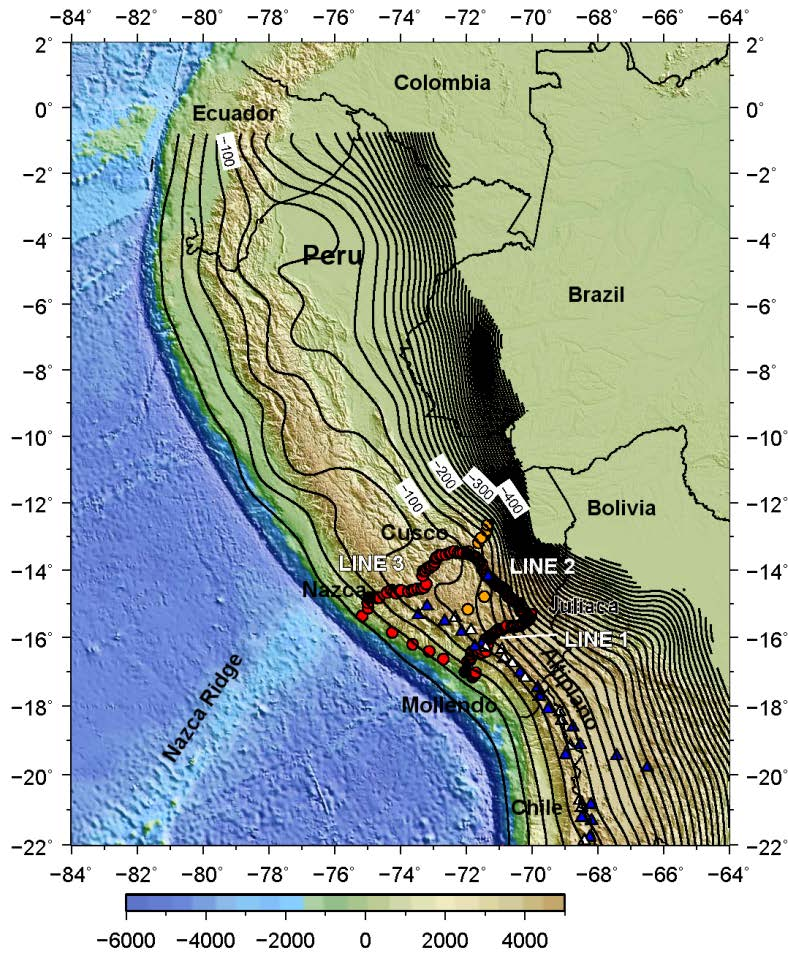


Figure 1.1. Topography and bathymetry map of Peru showing slab contours from the Slab 1.0 model. The seismic arrays are shown as red circles. Orange circles denote added stations from the CAUGHT/PULSE experiments. Dormant/active volcanoes are shown as blue/yellow triangles.

The purpose of the project is to clarify the structure beneath the arrays to learn more about the present state of the subduction system, compare the normal and flat slab regions, and study the nature of the transition between the two subduction regimes.

Overarching questions which stem from these observables are what are primary causes of flab slab subduction in Peru and what is the tectonic evolution of the area.

The array in the flat slab region is located near where the Nazca Ridge is presently subducting and can be useful in estimating the effect of the ridge on the subduction system. The thickened crust from subducting oceanic ridges, plateaus, and other such impactors has been suggested to be a possible cause or contributor to flat slab subduction by adding to the buoyancy of the subducting plate (Gutscher, Olivet, et al. 1999; Gutscher, Malavielle, et al. 1999, Gutscher et al. 2000; van Hunen et al. 2002a, 2002b, 2004; McGearry et al. 1985, and Rosenbaum and Mo 2011). This notion is supported by observations that many flat slab regions have corresponding buoyant impactors such as the Juan Fernandez ridge in Chile and the Carnegie Ridge in Ecuador. A difference between Peru and other flat slab regions is that the flat slab region in Peru is over 1500 km in length which is about three times the length of many other flat slab regions. The Nazca Ridge has been migrating south through time and is located near the southern end of the flat slab region but is not expected to have enough buoyancy to support the length of the flat slab region or keep the slab from returning to a normal dip angle in its wake.

The array in the normal subduction region intersects the present active volcanic arc which ends at the southern end of the flat segment where there is a volcanic gap. Gaps in volcanism are observable in many flat slab regions because the lack of asthenospheric wedge between the subducting and overlying plates inhibits partial melting (Gutcher, Malavielle, et al. 1999). A look at the migration of the volcanic arc through time provides information about the tectonic evolution of a region. For example when a steeply dipping slab begins to flatten, the arc is seen to advance or migrate inland away from the trench as is observed in Chile (Hascke 2002; Kay and Abbruzi 1996; Kay et al.

2005; Kay and Mpodozis 2002). As a flat slab begins to steepen again (or “roll back”), the volcanic arc is seen to move toward the trench which is thought to be happening in Mexico (Ferrari et al, 2001). In some areas both processes can be observed as the volcanic arc first migrates away from the trench and later migrates back to the trench as happened in western North America during the Laramide (Saleeby 2003). In Peru the volcanic arc was observed to move eastward before extinguishing (Soler and Bonhomme, 1990) and over time as the slab begins to steepen due to eclogitization and increasing pull from the already subducted material the arc will begin to migrate westward again.

The second chapter in this work presents results from “Line 1” running from Mollendo to Juliaca in the normal slab region where the slab is seen to be dipping at 30 degrees. The receiver function method is used to provide direct information about the structure beneath the stations. Signals are observed from the Moho at the base of the crust and the top of the subducting Nazca plate. One of the key observations is of a strong midcrustal positive impedance signal at 40 km depth beneath the eastern portion of the array where the Moho depth is observed to be around 70-75 km beneath the Altiplano. This is suggested to be a possible observation of the underthrusting of the Brazilian Shield which other authors have suggested underthrusts as far as the Eastern Cordillera (McQuarrie et al. 2005; Gubbels et al. 1993; Lamb and Hoke 1997; Beck and Zandt 2002). We suggest here that it underthrusts farther beneath southern Peru and even underlies a portion of the Altiplano. Such an observation has implications for the timing of uplift in the Altiplano. We suggest that the underthrusting of the Brazilian shield is more consistent with a gradual uplift model over the last 40 Ma rather than rapid uplift over the past 10 Ma caused by lithospheric delamination. Although such delamination and rapid uplift may

have occurred further south in the Andes in the Puna Plateau, we suggest that the dominant mechanisms for uplift in the Altiplano of southern Peru are crustal shortening accompanied by tectonic underthrusting from the Brazilian craton.

The third chapter presents results from “Line 2” and “Line 3” in the transition from normal to flat slab subduction and flat slab regions respectively. Line 2 shows the clearest signal from the midcrustal structure at 40 km depth. The shape of the slab is observed and is suggested to be a contortion rather than a tear in the slab. Results from Line 3 show the slab flattening out almost horizontally beneath the Altiplano at a depth of about 100 km. Results from this array are compared to the results from Line 1 in the normal subduction region.

The fourth chapter presents further details of the methods used including methods which are not presented in the papers. The results from this project are part of the PeruSE (Peru Seismic Experiment) which began with field work and installation of broadband seismic stations in 2008. The details of installation and seismic equipment used are presented. The second array was installed and began collecting data in late 2009 while half of the third array began collecting data in late 2010. The installation of the third array was completed in 2011. After the collection of seismic data, teleseismic events were analyzed with distances greater than 30 degrees and magnitudes greater than 5.8. The receiver function method was used to provide more information about the structure beneath the stations using deconvolution in the frequency domain. Both these results and results using iterative time domain deconvolution are described. Although most receiver function studies focus on P waves which convert to S waves at impedance contrasts, the

great distance of many events from Peru made it useful to be able to include PP and PKP phases. Results are compared using the various P-based phases to show the compatibility of the receiver functions using the different phases. In addition to P, PP, and PKP phases, S wave receiver functions were also attempted which have been used to look for the lithosphere-asthenosphere boundary (LAB). Multiple receiver functions for each station from similar azimuthal directions are stacked to obtain estimates for Moho depth and V_p/V_s from the maximum summation of receiver functions at the time of the converted phase and multiples. Although most of the analysis is done with radial receiver function, transverse receiver functions were also analyzed. The presence of energy on the transverse component can be suggestive of either a dipping interface or anisotropy. The structure beneath the stations, including interfaces such as the Moho and subducting oceanic crust can be clarified by plotting the amplitudes of receiver functions in cross section using methods such as backprojecting rays and CCP (common conversion point stacking). The backprojection method assumes an approximately linear ray path and plots the amplitudes of receiver functions from the direction in which the energy arrived so that each point along the receiver function is at the correct depth and distance from the station. The amplitude at any given point in the image is an average of the amplitudes of receiver functions which pass through that point. The CCP method is similar except it calculates the piercing point of the ray with the expected depth of the Moho. All other rays which pass through this region are stacked and the resulting stacks are plotted. The receiver function methods use an average P wave velocity model. Simple 2D velocity models are tested using finite difference modeling. Two different methods are used to model both teleseismic energy to produce synthetic receiver functions, and to model local

events allowing for the comparison of synthetic seismograms with data. Local events were also analyzed but further analysis of local earthquakes is an area for future study. In summary, the receiver function results shown in these chapters clarify the structure beneath southern Peru to elucidate the present state of the subduction system. Results are compared for the normal and flat slab regions which has implications for studying the causes of flat slab subduction. The transition from normal to flat slab subduction is also observed.

Chapter 1 References

- Barazangi, M., and B. L. Isacks (1976), Spatial distribution of earthquakes and subduction of the Nazca plate beneath South America, *Geology*, 4, 686–692.
- Beck, S., and G. Zandt (2002), The nature of orogenic crust in the Central Andes, *Journal of Geophysical Research*, 107, 2230.
- Ferrari, L., C. M. Petrone, and L. Francalanci (2001), Generation of oceanic-island basalt-type volcanism in the western Trans-Mexican volcanic belt by slab rollback, asthenosphere infiltration, and variable flux melting, *Geology*, 29 (6), 507-510.
- Gubbels, T., B. Isacks, and E. Farrar (1993), High-level surfaces, plateau uplift, and foreland development, Bolivian central Andes, *Geology*, 21, 695–698.
- Gutscher, M., J. Malavielle, S. Lallemand, J.-Y. Collot (1999), Tectonic segmentation of the North Andean margin: Impact of the Carnegie Ridge collision, *Earth and Planetary Science Letters* 168, 255–270.
- Gutscher, M., J. Olivet, D. Aslanian, J. Eissen, and R. Maury (1999), The “lost Inca Plateau”: Cause of flat subduction beneath Peru?, *Earth and Planetary Science Letters*,

- 171 (3), 335–341.
- Gutscher, M., W. Spakman, H. Bijwaard, and E. Engdahl (2000), Geodynamics of flat subduction: Seismicity and tomographic constraints from the Andean margin, *Tectonics*, 19 (5), 814–833.
 - Haschke M. (2002), Evolutionary geochemical patterns of Late Cretaceous to Eocene arc magmatic rocks in North Chile: implications for Archean crustal growth, EGU Stephan Mueller Special Publication Series, 2, 207–218.
 - Kay, S. M. & J. M. Abbruzzi (1996), Magmatic evidence for Neogene lithospheric evolution of the central Andean “flat-slab” between 30° S and 32° S, *Tectonophysics*, 259, 15–28.
 - Kay, S. M., E. Godoy, & A. Kurtz (2005), Episodic arc migration, crustal thickening, subduction erosion, and magmatism in the south-central Andes, *GSA Bulletin*, 117, (1/2), 67–88.
 - Kay, S. M. & C. Mpodozis (2002), Magmatism as a probe to the Neogene shallowing of the Nazca plate beneath the modern Chilean flat-slab, *Journal of South American Earth Sciences*, 15, 39–57.
 - Lamb, S., and L. Hoke (1997), Origin of the high plateau in the Central Andes, Bolivia, South America, *Tectonics*, 16 (4), 623–649.
 - McGearry S., A. Nur, and Z. Ben-Avraham (1985), Spatial gaps in arc volcanism: the effect of collision or subduction of oceanic plateaus, *Tectonophysics*, 119, 195–221.
 - McQuarrie, N., B. Horton, G. Zandt, S. Beck, and P. DeCelles (2005), Lithospheric evolution of the Andean fold-thrust belt, Bolivia, and the origin of the central Andean plateau, *Tectonophysics*, 399, 15–37.

- Rosenbaum, G., and W. Mo (2011), Tectonic and magmatic responses to the subduction of high bathymetric relief, *Gondwana Research*, 19, 571–582.
- Saleeby, J. (2003), Segmentation of the Laramide Slab—evidence from the southern Sierra Nevada region, *GSA Bulletin*, 115, 6, 655–668.
- Soler, P. & M. Bonhomme (1990), Relation of magmatic activity to plate dynamics in central Peru from Late Cretaceous to present, Geological Society of America, Special paper 241.
- van Hunen, J., A. van den Berg, and N. Vlaar (2002a), The impact of the South American plate motion and the Nazca Ridge subduction on the flat subduction below South Peru, *Geophysical Research Letters*, 29 (14).
- van Hunen, J., A. van den Berg, and N. Vlaar (2002b), On the role of subducting oceanic plateaus in the development of shallow flat subduction, *Tectonophysics*, 352, 317–333.
- van Hunen, J., A. van den Berg, N. Vlaar (2004), Various mechanisms to induce present-day shallow flat subduction and implications for the younger Earth: a numerical parameter study, *Physics of the Earth and Planetary Interiors* , 146, 179–194.